The Cryosphere Discuss., 7, 1119–1139, 2013
www.the-cryosphere-discuss.net/7/1119/2013/
doi:10.5194/tcd-7-1119-2013

The Cryosphere Discussions
Open Access

Recent mass balance of Purogangri ice cap, central Tibetan Plateau, by means of differential X-band SAR interferometry

N. Neckel, A. Braun, J. Kropáček, and V. Hochschild

Institute of Geography, University of Tübingen, Rümelinstr. 19–23, 72070 Tübingen, Germany

Received: 11 February 2013 – Accepted: 7 March 2013 – Published: 21 March 2013

Correspondence to: N. Neckel (niklas.neckel@uni-tuebingen.de)

Published by Copernicus Publications on behalf of the European Geosciences Union.

Abstract

Due to their remoteness, altitude and harsh climatic conditions, little is known about the glaciological parameters of ice caps on the Tibetan Plateau (TP). This study presents an interferometrical approach aiming at surface elevation changes of Purogangri ice cap, located on the central TP. Purogangri ice cap covers an area of 397 ± 9.7 km^2 and is the largest ice cap on the TP. Its behavior is determined by dry and cold continental climate suggesting a polar-type glacier regime. We employed data from the actual TerraSAR-X mission and its add-on for Digital Elevation Measurements (TanDEM-X) and compare it with elevation data from the Shuttle Radar Topography Mission (SRTM). These datasets are ideal for this approach as both datasets feature the same wavelength of 3.1 cm and are available at a fine grid spacing. Similar snow conditions can be assumed since the data were acquired in early February 2000 and late January 2012. The trend in glacier extent was extracted using a time series of Landsat data. Our results show a balanced mass budget for the studied time period which is in agreement with previous studies. Additionally, we detected an exceptional fast advance of one glacier tongue in the eastern part of the ice cap between 1999 and 2011.

1 Introduction

The TP, also known as the third pole, stores the world's largest amount of perennial surface ice outside the Arctic and Antarctic. Information whether this ice is losing or gaining mass is a valuable indicator to understand the climate variability on the TP (Yao et al., 2012). This is of high importance as direct measurements of climatic parameters are sparse, especially in the central part of the TP (Thompson et al., 2006). In this study we take a closer look at the recent mass balance of Purogangri ice cap, Tibet's largest ice field (Shi et al., 2009). Purogangri ice cap is located at 33°05′ N, 89°10′ E in the continental westerly-dominated north-central part of the TP (Thompson et al., 2006). Due to its remoteness and high altitude of 5800 m a.s.l on average, field work at

Purogangri ice cap would involve high costs, large logistical efforts and great physical strain. Therefore, remote sensing is a promising alternative to conduct mass balance measurements of this ice cap.

In this study we estimate the mass balance by geodetic means. In general, the geodetic mass balance is calculated by subtracting datasets of glacier surface elevation acquired at different times (e.g. Rignot et al., 2003; Kääb, 2008; Haug et al., 2009; Bolch et al., 2011). For Purogangri ice cap two such datasets are available. The ice cap was almost completely mapped by X-band SAR interferometry (InSAR) in February 2000 during the Shuttle Radar Topography Mission (SRTM). Almost exactly 12 years later, on 26 January 2012 the ice cap was mapped by single-pass X-band InSAR from TerraSAR-X and its add-on for Digital Elevation Measurements (TanDEM-X) (Krieger et al., 2007). Utilizing these datasets we followed two different approaches to estimate the geodetic mass balance of Purogangri ice cap between 2000 and 2012. At first we employed differential synthetic aperture radar interferometry (DInSAR). In this approach differencing starts from the interferometric phase rather than from absolute surface elevations. In order to validate the DInSAR derived estimate, elevation changes were also derived from absolute surface elevations employing common DEM differencing.

2 Data

2.1 Shuttle Radar Topography Mission

The Shuttle Radar Topography Mission (SRTM) was conducted from 11 to 22 February 2000 in order to derive a near-global DEM (Rabus et al., 2003; Farr et al., 2007). For this purpose data from C- and X-band SAR were acquired. In this study we use the X-band DEM, which was processed at the German Aerospace Center (DLR). The X-band system operated at a wavelength of 3.1 cm with a swath width of ∼ 45 km on the ground (Rabus et al., 2003). The latter leads to larger data gaps in the DEM. Fortunately,

Purogangri ice cap is almost completely covered by the dataset (Fig. 1). The SRTM-X DEM is freely available to the public and can be downloaded via DLR's Earth Observation on the WEB (EOWEB) portal. The original DEM is sampled to a 25 m × 25 m grid and is referenced to the WGS84 ellipsoid. We found a standard deviation of 2.27 m compared to data acquired by the Geoscience Laser Altimeter System (GLAS) carried on-board the Ice Cloud and Elevation Satellite (ICESat) in off-glacier terrain (see Fig. 1 for ICESat footprint locations). These values are in agreement with a standard deviation of 2.67 m estimated by Hoffmann and Walter (2006) who compared the DEM with Global Positioning System (GPS) measurements in Germany.

2.2 TerraSAR-X and its add-on for Digital Elevation Measurements (TanDEM-X)

TerraSAR-X was launched in June 2007 followed by its twin satellite TanDEM-X in June 2010. The two satellites are flying in a unique helical formation acting as a single-pass InSAR system with a flexible baseline configuration (Krieger et al., 2007). The main goal of the TanDEM-X mission is the generation of a global consistent DEM with a 12 m × 12 m grid posting and a vertical accuracy of < 2 m (Moreira et al., 2004).

In this study we employed experimental Coregistered Single look Slant range Complex (CoSSC) products acquired in bistatic InSAR stripmap mode on 26 January 2012. The perpendicular baseline of the used data pair is estimated with 155 m. For the derived DEM we found a standard deviation of 1.0 m compared to ICESat measurements, which is well within the mission requirements. Next to the tandem acquisition we employed two TerraSAR-X images acquired on 2 and 13 August 2011 (Table 1).

2.3 Landsat

In order to compare the interferometrical derived results with changes in glacier extend we utilized six Landsat Enhanced Thematic Mapper Plus (ETM+) and two Landsat Thematic Mapper (TM) scenes (Table 1). We employed the orthorectified level T1 product provided by the United States Geological Survey (USGS). No horizontal shift

amongst the Landsat imagery with respect to the SRTM-X DEM was observed. In order to reduce data gaps induced by scanline errors in the 2012 ETM+ data we combined two ETM+ scenes acquired in September 2012 (e.g. Chen et al., 2011). To enhance the spatial resolution of the Landsat ETM+ scenes to 15 m, pan-sharpening employing principal component analysis was performed.

3 Methods

3.1 Delineation of ice

In order to measure any glaciological parameter the delineation of the ice body is an essential step. We conducted an unsupervised 2-class classification of the 2000 and 2012 pan-sharpened Landsat ETM+ images to classify the ice body for the years 2000 and 2012 respectively. Choosing only 2 classes resulted in a general determination of on-glacier and off-glacier areas. Due to snow covered mountain ridges and remains of snow avalanches, the derived glacier masks were adjusted manually according to the Global Land Ice Measurements from Space (GLIMS) standards (Rau et al., 2005). In consequence of occasional cloud cover in the ETM+ data of 2012 we employed an additional coherence image of a 11 day repeat-pass of TerraSAR-X acquired on 2 and 13 August 2011 (Table 1). Due to the short wavelength of TerraSAR-X (3.1 cm) and the changing surface characteristics of the ice cap (e.g. precipitation, wind drift, melting, freezing) a low coherence was calculated for ice covered areas. Ice divides were estimated on the basis of watersheds extracted from the SRTM-X DEM utilizing the *r.watershed* tool implemented in the GRASS GIS software (GRASS Development Team, 2012). For an error estimate of the resulting glacier masks parts of the ice cap were independently digitized from the TerraSAR-X coherence image and compared to the 2012 glacier extents.

3.2 Glacier elevation changes

The interferometric phase of a single-pass interferogram may be described by

$$\Delta\phi_{ij} = \Delta\phi_{\text{orbit}} + \Delta\phi_{\text{topo}} + \Delta\phi_{\text{atm}} + \Delta\phi_{\text{scat}} \quad (1)$$

where $\Delta\phi_{ij}$ is the difference of phases ϕ_i and ϕ_j simultaneously acquired by two SAR antennas. As the baseline of a single-pass system is usually small (e.g. 59.9 m for SRTM-X) and the data is acquired simultaneously same atmospheric conditions can be assumed for both antennas, which sets the atmospheric contribution $\Delta\phi_{\text{atm}}$ in Eq. (1) to zero. The same applies for $\Delta\phi_{\text{scat}}$, which describes the phase difference due to different scattering on the ground (Rabus et al., 2003). This only leaves $\Delta\phi_{\text{orbit}}$, which is the phase difference induced by the different acquisition geometry of the SAR sensors, and $\Delta\phi_{\text{topo}}$, which describes the phase difference induced by topography[1]. In this study we applied a differential approach (DInSAR), which means the subtraction of two interferograms acquired at two different times (e.g. Kwok and Fahnestock, 1996). In our case this is described by

$$\Delta\phi'_{\text{diff}} = \Delta\phi_{\text{TanDEM}} - \Delta\phi_{\text{SRTM}} \quad (2)$$

where $\Delta\phi_{\text{TanDEM}}$ is the interferometric phase of the TerraSAR-X/TanDEM-X (TSX/TDX) acquisition and $\Delta\phi_{\text{SRTM}}$ is the interferometric phase of the SRTM-X acquisition. As the raw interferometric data of the SRTM is not available, $\Delta\phi_{\text{SRTM}}$ was simulated from DEM data using the satellite geometry and baseline model of the TSX/TDX pass from 26 January 2012. Since the same satellite geometry and baseline model was used for both interferograms, $\Delta\phi'_{\text{diff}}$ is solely based on changes in $\Delta\phi_{\text{topo}}$ between data acquisitions. To calculate absolute height values from the difference interferogram 20 Ground Control Points (GCP's) were selected manually in off-glacier regions. The differential

[1] For further reading on InSAR the reader is referred to Massonnet and Feigl (1998) and Rosen et al. (2000).

phase was set to zero at these points as no changes are assumed in this regions between data acquisitions.

To archive accurate results precise offset registration and fitting between both datasets is mandatory. Therefore, we calculated a DEM from the TSX/TDX interferogram and sampled it to a 25 m × 25 m grid, i.e. the same grid posting as the SRTM-X DEM. In the interferometric processing of the TSX/TDX DEM we observed an artificial linear phase ramp presumably related to an inaccurate flat earth estimate. The linear phase ramp could be removed by an additional baseline refinement based on off-glacier phase values from the differential interferogram. For the calculation of absolute heights GCP's were obtained from the respective pixel locations in the SRTM-X DEM. In order to calculate horizontal offsets between both datasets two SAR images were simulated from the DEM's using the orbital parameters of the TSX/TDX pass (e.g. Kropáček et al., 2012). Offsets were calculated using cross correlation optimization of the simulated SAR images employing the *offset_pwrm* module implemented in the GAMMA SAR and interferometric processing software (e.g. Werner et al., 2000). These offsets were used to refine the horizontal data registration via a refined geocoding lookup table.

In order to validate the DInSAR derived elevation changes we also constructed a difference map from absolute surface elevations by differencing of the spatially adjusted DEM's.

For the estimation of the random contribution to the overall error we used the standard error S_ε in off-glacier regions between both interferometric datasets which is defined by

$$S_\varepsilon = \frac{\sigma}{\sqrt{n}} \tag{3}$$

where σ is the standard deviation of non-glacier elevation differences and n is the number of non-glacier grid cells (either for the DInSAR derived estimate or for the absolute estimate). Utilizing all non-glacier grid cells on a 25 m × 25 m gird would lead to an underestimation of S_ε due to spatial autocorrelation. By analysing semivariograms we

detected a decorrelation distance of ∼ 100 m. As a consequence we reduced the grid spacing of non-glacier grid cells to 200 m × 200 m.

According to the law of error propagation the error in elevation change is estimated by

$$e = \sqrt{(S_\varepsilon)^2 + (\bar{x})^2} \tag{4}$$

where the mean $\bar{x}$ of non-glacier elevation differences contributes as the systematic part of the overall error.

In order to convert elevation changes to mass balances knowledge of the materials density is required. Here we create two scenarios. Following Sorge's law (Bader, 1954) we assume an unchanged density profile and used an ice density of 900 kg m^{-3} (e.g. Paterson, 1994; Berthier et al., 2007, 2010; Bolch et al., 2011) for the entire glacier area considering that only ice is losing or gaining mass. In the second scenario we separated the ice cap into an accumulation and an ablation area at the zero contour line of on-glacier elevation changes (black dot in Fig. 3, upper plot). Here we assume area weighted densities of 600 kg m^{-3} in the accumulation area and of 900 kg m^{-3} in the ablation area (Berthier et al., 2007; Kääb et al., 2012; Neckel et al., 2013).

4 Results

Similar to Lei et al. (2012) who estimated surface elevation changes of Purogangri ice cap between 1974 and 2000 we found predominant surface lowering in glacier tongue regions and glacier thickening in the interior of the ice cap (Fig. 2). This is also evident from Fig. 3 (upper plot) where negative elevation changes are correlated to altitudes lower 5750 m a.s.l. and positive elevation changes are found at higher altitudes. The lower part of Fig. 3 suggests no elevation-dependent bias in off-glacier regions making an artificial elevation dependency for on-glacier elevation changes unlikely.

Altogether our results suggest a balanced mass budget for the last 12 years for the observed part of the ice cap. Following Sorge's law we calculated a mean mass budget

of +0.01 ± 0.36 m w.e. from the DInSAR approach and of +0.3 ± 0.05 m w.e. from the DEM differencing. For the second density scenario we calculated a mean mass budget of −0.65 ± 0.3 m w.e. from the DInSAR approach and of −0.44 ± 0.04 m w.e. from the DEM differencing for the observed time period. Also the changes in glacier area suggest a balanced glacier regime between 2000 and 2012. For October 2000 we estimated a glacier area of 398 ± 9.7 km^2 while for September 2012 we calculated a glacier area of 397 ± 9.7 km^2, which indicates no significant changes. These findings are in agreement with Yao et al. (2012) and Neckel et al. (2013) who estimated balanced mass changes in the north-western part of the TP for a similar time period ~~on contrary to the remaining parts of the TP.~~ Also Lei et al. (2012) found that Purogangri ice cap retreats at a much slower rate than other glaciers on the TP.

Prominent positive elevation changes were found for one glacier tongue in the eastern part of the ice cap (Fig. 4). Between August 1999 and September 2011 the glacier terminus advanced by 515 m at an average rate of 43 m per year.

5 Discussion

Several studies exist which estimate the mass balance of glaciers and ice caps from remotely sensed datasets in different parts of the world by DEM differencing (e.g. Rignot et al., 2003; Kääb, 2008; Haug et al., 2009; Bolch et al., 2011). In this study elevation changes were calculated in two different ways. The first approach makes use of the interferometric phase of a differential interferogram, while the second approach starts from absolute surface elevation values. As no filter was applied in the latter the result shows more data noise than the DInSAR derived map of elevation changes which uses adaptive filtering (Goldstein and Werner, 1998) on the differential interferogram prior to phase unwrapping. This is evident from the histograms shown in Fig. 2 and from the off-glacier 1-σ values of 4.7 m for the DInSAR approach and of 7.3 m for the DEM differencing used in Eq. (3). Another advantage of the the DInSAR approach is the removal of residual phase ramps related to the orbit geometry by subtracting

the simulated interferogram. However in this study the overall error is smaller for the DEM differencing because of a smaller systematic error component. Altogether both approaches show a quite similar pattern.

In both difference maps shown in Fig. 2 we found prominent linear features running from south-west to north-east. Similar pattern were found by Nuth and Kääb (2011) and Iwasaki (2011) in the cross-track direction when differencing two spatially adjusted Advance Spaceborne Emission and Reflection radiometer (ASTER) DEMs which they attributed to satellite attitude jitter. Figure 5 shows a profile taken along the black line shown in Fig. 2b. The profile follows approximately the along-tack direction of the SRTM acquisition suggesting attitude jitter of the space shuttle. Mostly these jitter-like patterns range between −5 m and +5 m (Fig. 5) which is within the range of on-glacier elevation changes making them only visible in off-glacier regions.

Penetration effects of SAR signals in snow and ice are widely discussed in the literature (e.g. Rignot et al., 2001; Gardelle et al., 2012a). The uncertainty induced by these effects are difficult to quantify when comparing InSAR derived DEM's with other datasets (e.g. Sauber et al., 2005; Berthier et al., 2006; Nuth and Kääb, 2011). The great advantage in this study is that the used datasets were acquired at the same wavelength at nearly the same time of the year leading to unbiased results.

Our results suggest a balanced glacier regime for Purogangri ice cap between 2000 and 2012 which is in agreement with Neckel et al. (2013) who found a slightly positive trend in mass balance for Zangser Kangri ice cap between 2003–2009 located ~ 300 km to the north-west. However this behavior is contrary to the remaining parts of the TP where glacier mass balances are negative (Yao et al., 2012; Neckel et al., 2013). The balanced mass budget of Purogangri ice cap may be related to the same mechanism as the frequently mentioned Karakoram Anomaly (e.g. Hewitt, 2005; Gardelle et al., 2012b). A possible explanation could be a compensation of the temperature driven melt-off due to an increase of precipitation in high altitudes. This is in agreement with Li et al. (2011) who showed a significant increase in annual temperature and

precipitation between 1961–2008 from meteorological station measurements on the TP.

We found negative elevation changes in glacier tongue regions except for one glacier in the eastern part of the ice cap. This glacier shows thickening at the terminus while neg[illegible] values are found further up the glacier (Fig. 4). These areas could be construed as reservoir and receiving areas of a surging glacier (Paterson, 1994), however the relatively slow velocity and long time period of constant glacier advance speaks against a hypothesized surging event.

6 Conclusions

In this study we estimated the recent mass budget for large parts of Purogangri ice cap by geodetic means. We employed SRTM elevation data from February 2000 and compared it with TSX/TDX data acquired in January 2012. Very similar results were achieved by a DInSAR based approach and DEM differencing, however the DInSAR approach showed lesser data noise. We estimated positive elevation changes in the accumulation area of the ice cap while negative elevation changes were found in glacier tongue regions, except for one advancing glacier in the eastern part of the ice cap. The overall mass budget between 2000 and 2012 is close to zero, which is in agreement with previous studies. Our findings show that the observed part of Purogan[illegible]e cap did not retreat in the last 12 years, which is contrary to other Tibetan glaciers.

Acknowledgements. This study has been carried out within the framework of the German Federal Ministry of Education and Research (BMBF) Programme “Central Asia – Monsoon Dynamics and Geo-Ecosystems” (CAME) within the WET project (“Variability and Trends in Water Balance Components of Benchmark Drainage Basins on the Tibetan Plateau”) under the code 03G0804A. SRTM-X, TerraSAR-X and TanDEM-X data were provided by the German Aerospace Center (DLR) under project ID HYD0534 and XTI_GLAC1054 respectively. All SAR processing was done with the GAMMA SAR and interferometric processing software. Thanks to U. Wegmüller, W. Rack and V. Helm for some hints and discussion in the processing of the TSX/TDX DEM.

References

Bader, H.: Sorge’s law of densification of snow on high polar glaciers, J. Glaciol., 2, 319–323, 1954. 1126

Berthier, E., Arnaud, Y., Vincent, C., and Remy, F.: Biases of SRTM in high-mountain areas: Implications for the monitoring of glacier volume changes, Geophys. Res. Lett., 33, doi:10.1029/2006GL025862, 2006. 1128

Berthier, E., Arnaud, Y., Kumar, R., Ahmad, S., Wagnon, P., and Chevallier, P.: Remote sensing estimates of glacier mass balances in the Himachal Pradesh (Western Himalaya, India), Remote Sens. Environ., 108, 327–338, doi:10.1016/j.rse.2006.11.017, available at: http://www.sciencedirect.com/science/article/pii/S0034425706004809, 2007. 1126

Berthier, E., Schiefer, E., Clarke, G. K. C., Menounos, B., and Remy, F.: Contribution of Alaskan glaciers to sea-level rise derived from satellite imagery, Nat. Geosci., 3, 92–95, doi:10.1038/ngeo737, 2010. 1126

Bolch, T., Pieczonka, T., and Benn, D. I.: Multi-decadal mass loss of glaciers in the Everest area (Nepal Himalaya) derived from stereo imagery, The Cryosphere, 5, 349–358, doi:10.5194/tc-5-349-2011, 2011. 1121, 1126, 1127

Chen, J., Zhu, X., Vogelmann, J. E., Gao, F., and Jin, S.: A simple and effective method for filling gaps in Landsat ETM+ SLC-off images, Remote Sens. Environ., 115, 1053–1064, doi:10.1016/j.rse.2010.12.010, available at: http://www.sciencedirect.com/science/article/pii/S0034425710003482, 2011. 1123

Farr, T. G., Rosen, P. A., Caro, E., Crippen, R., Duren, R., Hensley, S., Kobrick, M., Paller, M., Rodriguez, E., Roth, L., Seal, D., Shaffer, S., Shimada, J., Umland, J., Werner, M., Oskin, M., Burbank, D., and Alsdorf, D.: The Shuttle Radar Topography Mission, Rev. Geophys., 45, RG2004, doi:10.1029/2005RG000183, 2007. 1121

Gardelle, J., Berthier, E., and Arnaud, Y.: Impact of resolution and radar penetration on glacier elevation changes computed from DEM differencing, J. Glaciol., 58, 419–422, 2012a. 1128

Gardelle, J., Berthier, E., and Arnaud, Y.: Slight mass gain of Karakoram glaciers in the early twenty-first century, Nat. Geosci., 5, 322–325, doi:10.1038/ngeo1450, 2012b. 1128

Goldstein, R. M. and Werner, C. L.: Radar interferogram filtering for geophysical applications, Geophys. Res. Lett., 25, 4035–4038, doi:10.1029/1998GL900033, 1998. 1127

GRASS Development Team: Geographic Resources Analysis Support System (GRASS GIS) Software, Open Source Geospatial Foundation, USA, available at: http://grass.osgeo.org, 2012. 1123

Haug, T., Rolstad, C., Elvehoy, H., Jackson, M., and Maalen-Johansen, I.: Geodetic mass balance of the western Svartisen ice cap, Norway, in the periods 1968–1985 and 1985–2002, Ann. Glaciol., 50, 119–125, doi:10.3189/172756409787769528, available at: http://www.ingentaconnect.com/content/igsoc/agl/2009/00000050/00000050/art00017, 2009. 1121, 1127

Hewitt, K.: The Karakoram anomaly? Glacier expansion and the "Elevation Effect," Karakoram Himalaya, Mt. Res. Dev., 25, 332–340, doi:10.1659/0276-4741(2005)025[0332:TKAGEA]2.0.CO;2, 2005. 1128

Hoffmann, J. and Walter, D.: How complementary are SRTM-X and -C band digital elevation models?, Photogramm. Eng. Rem. S., 72, 261–268, 2006. 1122

Iwasaki, A.: Detection and estimation of satellite attitude jitter using remote sensing imagery, in: Advances in Spacecraft Technologies, InTech, 257–272, doi:10.5772/14402, 2011. 1128

Kääb, A.: Glacier volume changes using ASTER satellite stereo and ICESat GLAS laser altimetry. A test study on Edgeøya, Eastern Svalbard, IEEE T. Geosci. Remote, 46, 2823–2830, 2008. 1121, 1127

Kääb, A., Berthier, E., Nuth, C., Gardelle, J., and Arnaud, Y.: Contrasting patterns of early twenty-first-century glacier mass change in the Himalayas, Nature, 488, 495–498, doi:10.1038/nature11324, 2012. 1126

Krieger, G., Moreira, A., Fiedler, H., Hajnsek, I., Werner, M., Younis, M., and Zink, M.: TanDEM-X: a satellite formation for high-resolution SAR interferometry, IEEE T. Geosci. Remote, 45, 3317–3341, doi:10.1109/TGRS.2007.900693, 2007. 1121, 1122

Kropáček, J., De Grandi, G., and Rauste, Y.: Geo-referencing of continental-scale JERS-1 SAR mosaics based on matching homologous features with a digital elevation model: theory and practice, Int. J. Remote Sens., 33, 2413–2433, doi:10.1080/01431161.2011.609843, available at: http://www.tandfonline.com/doi/abs/10.1080/01431161.2011.609843, 2012. 1125

Kwok, R. and Fahnestock, M. A.: Ice sheet motion and topography from radar interferometry, IEEE T. Geosci. Remote, 34, 189–200, 1996. 1124

Lei, Y., Yao, T., Yi, C., Wang, W., Sheng, Y., Li, J., and Joswiak, D.: Glacier mass loss induced the rapid growth of Linggo Co on the central Tibetan Plateau, J. Glaciol.,

58, 177–184, doi:10.3189/2012JoG11J025, available at: http://www.ingentaconnect.com/content/igsoc/jog/2012/00000058/00000207/art00015, 2012. 1126, 1127

Li, Z., He, Y., An, W., Song, L., Zhang, W., Catto, N., Wang, Y., Wang, S., Liu, H., Cao, W., Theakstone, W. H., Wang, S., and Du, J.: Climate and glacier change in southwestern China during the past several decades, Environ. Res. Lett., 6, 24, available at: http://stacks.iop.org/1748-9326/6/i=4/a=045404, 2011. 1128

Massonnet, D. and Feigl, K. L.: Radar interferometry and its application to changes in the Earth's surface, Rev. Geophys., 36, 441–500, doi:10.1029/97RG03139, 1998. 1124

Moreira, A., Krieger, G., Hajnsek, I., Hounam, D., Werner, M., Riegger, S., and Settelmeyer, E.: TanDEM-X: a TerraSAR-X add-on satellite for single-pass SAR interferometry, Int. Geosci. Remote Se., 2, 1000–1003, doi:10.1109/IGARSS.2004.1368578, 2004. 1122

Neckel, N., Kropáček, J., Bolch, T., and Hochschild, V.: Glacier elevation changes on the Tibetan Plateau between 2003 and 2009 derived from ICESat measurements, J. Geophys. Res., under review, 9, 2013. 1126, 1127, 1128

Nuth, C. and Kääb, A.: Co-registration and bias corrections of satellite elevation data sets for quantifying glacier thickness change, The Cryosphere, 5, 271–290, doi:10.5194/tc-5-271-2011, 2011. 1128

Paterson, W.: The Physics of Glaciers, 3rd edn., Pergamon, New York, 1994. 1126, 1129

Rabus, B., Eineder, M., Roth, A., and Bamler, R.: The shuttle radar topography mission – a new class of digital elevation models acquired by spaceborne radar, ISPRS J. Photogramm., 57, 241–262, doi:10.1016/S0924-2716(02)00124-7, available at: http://www.sciencedirect.com/science/article/pii/S0924271602001247, 2003. 1121, 1124, 1134

Rau, F., Mauz, F., Vogt, S., Khalsa, S., and Raup, B.: Illustrated GLIMS Glacier Classification Manual, NSIDC, 2005. 1123

Rignot, E., Echelmeyer, K., and Krabill, W.: Penetration depth of interferometric synthetic-aperture radar signals in snow and ice, Geophys. Res. Lett., 28, 3501–3504, doi:10.1029/2000GL012484, 2001. 1128

Rignot, E., Rivera, A., and Casassa, G.: Contribution of the Patagonia icefields of South America to sea level rise, Science, 302, 434–437, doi:10.1126/science.1087393, available at: http://www.sciencemag.org/content/302/5644/434.abstract, 2003. 1121, 1127

Rosen, P., Hensley, S., Joughin, I., Li, F., Madsen, S., Rodriguez, E., and Goldstein, R.: Synthetic aperture radar interferometry, Proc. IEEE, 88, 333–382, doi:10.1109/5.838084, 2000. 1124

Sauber, J., Molnia, B., Carabajal, C., Luthcke, S., and Muskett, R.: Ice elevations and surface change on the Malaspina Glacier, Alaska, Geophys. Res. Lett., 32, L23S01, doi:10.1029/2005GL023943, 2005. 1128

Shi, Y., Liu, C., and Kang, E.: The glacier inventory of China, Ann. Glaciol., 50, 1–4, doi:10.3189/172756410790595831, available at: http://www.ingentaconnect.com/content/igsoc/agl/2010/00000050/00000053/art00001, 2009. 1120

Thompson, L. G., Yao, T., Davis, M. E., Mosley-Thompson, E., Mashiotta, T. A., Lin, P.-N., Mikhalenko, V. N., and Zagorodnov, V. S.: Holocene climate variability archived in the Puruogangri ice cap on the central Tibetan Plateau, Ann. Glaciol., 43, 61–69, doi:10.3189/172756406781812357, available at: http://www.ingentaconnect.com/content/igsoc/agl/2006/00000043/00000001/art00010, 2006. 1120

Werner, C., Wegmüller, U., Strozzi, T., and Wiesmann, A.: GAMMA SAR and Interferometric Processing Software, in: ERS – ENVISAT Symposium, Gothenburg, Sweden, 2000. 1125

Yao, T., Thompson, L., Yang, W., Yu, W., Gao, Y., Guo, X., Yang, X., Duan, K., Zhao, H., Xu, B., Pu, J., Lu, A., Xiang, Y., Kattel, D. B., and Joswiak, D.: Different glacier status with atmospheric circulations in Tibetan Plateau and surroundings, Nat. Clim. Change, 2, 663–667, doi:10.1038/nclimate1580, 2012. 1120, 1127, 1128

Table 1. Overview of satellite data and date of data acquisition. Perpendicular baseline, $B_\perp$ and satellite orbit are given for SAR acquisitions (footprints are shown in Fig. 1). For Landsat data path and row number is given next to the spatial resolution.

SAR sensor	date	$B_\perp$ (m)	orbit
SRTM-X	11–22 Feb 2000	155*	ascend.
TSX	2/13 Aug 2011	403	descend.
TSX/TDX	26 Jan 2012	155	ascend.
optical sensor	**date**	**path/row**	**res. (m)**
Landsat ETM+	25 Aug 1999	140/036	15
Landsat ETM+	07 Oct 2000	139/037	15
Landsat ETM+	28 Oct 2005	140/036	15
Landsat ETM+	16 Sep 2007	140/036	15
Landsat TM	15 Aug 2010	140/036	30
Landsat TM	19 Sep 2011	140/036	30
Landsat ETM+	13 Sep 2012	140/036	15
Landsat ETM+	29 Sep 2012	140/036	15

* In this study the baseline was simulated from the TSX/TDX pass, the original SRTM-X baseline is 59.9 m (Rabus et al., 2003).

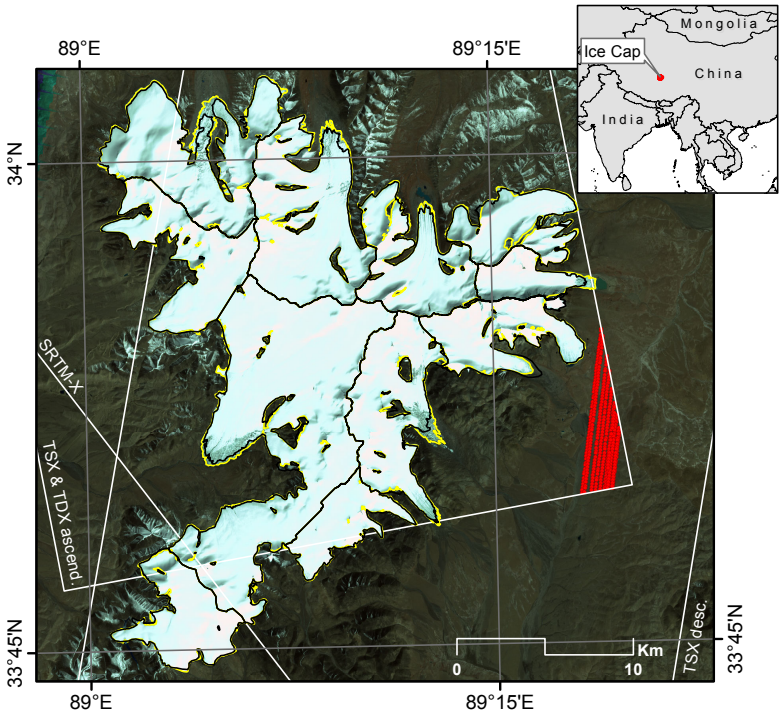

Fig. 1. Landsat ETM+ image acquired on 7 October 2000 of Purogangri ice cap overlayed by SAR image footprints and glacier outlines for the years 2000 (yellow) and 2012 (black). Bands 4, 3, and 2 are combined as red, green, and blue, respectively. ICESat footprints are indicated as small red dots.

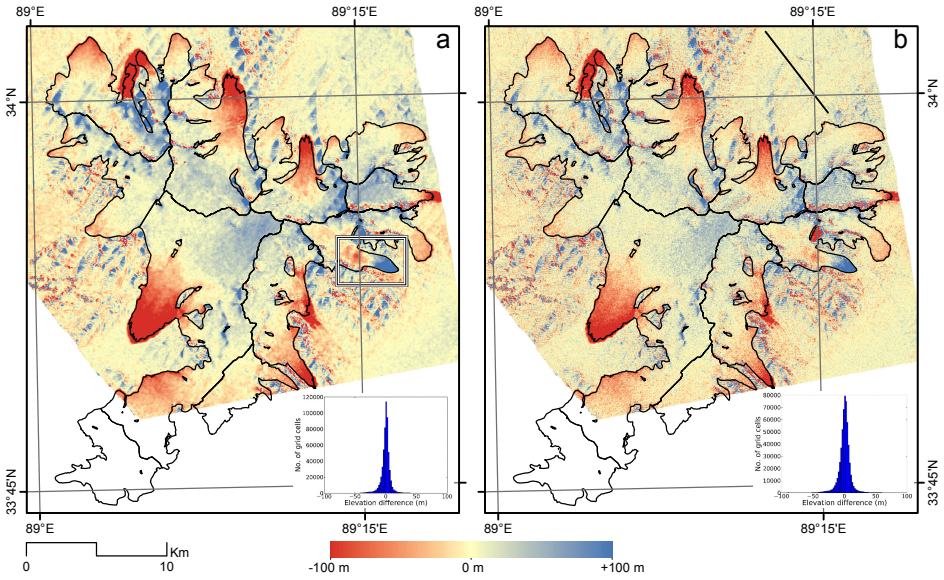

Fig. 2. Elevation changes of Purogangri ice cap between February 2000 and January 2012. **(a)** shows the difference map derived by DInSAR while **(b)** shows the difference map derived from absolute heights. Histograms show the on-glacier elevation differences.

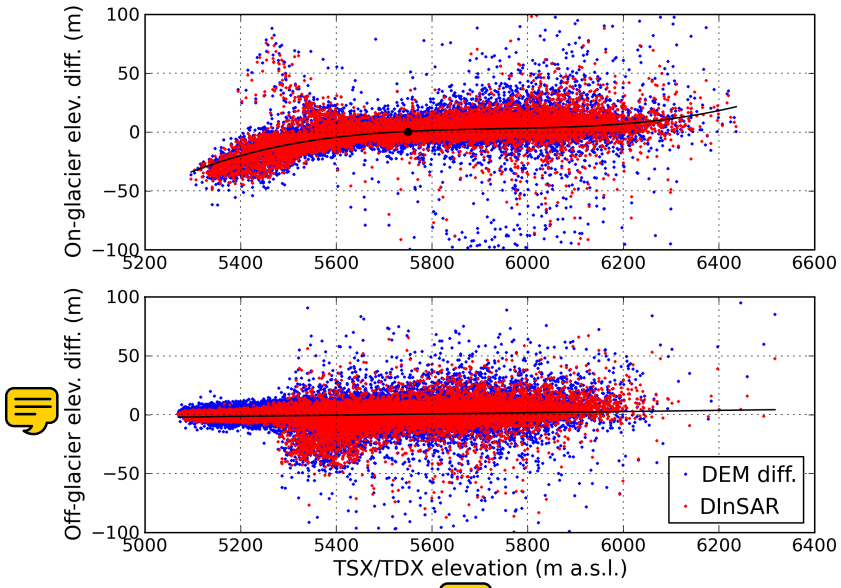

Fig. 3. Elevation changes of Purogangri ~~ice cap~~ as a function of TSX/TDX surface elevation (upper plot). Black dot shows the equilibrium line altitude (ELA) at ~ 5750 m a.s.l. No significant elevation-dependent bias is found in off-glacier regions (lower plot).

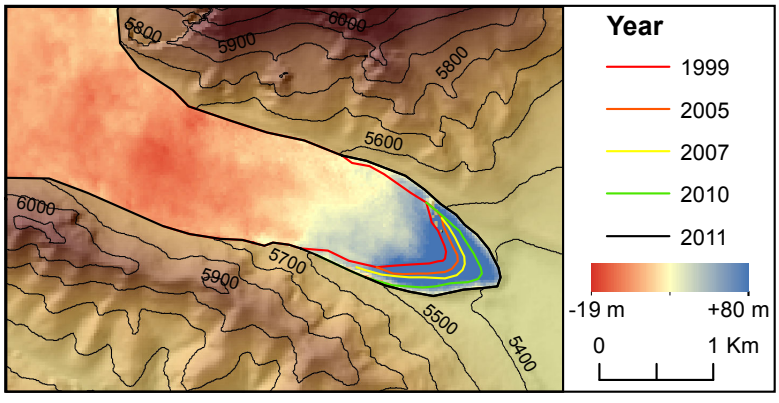

Fig. 4. Positive surface elevation changes in glacier tongue region. DInSAR derived surface elevation changes are color-coded. In the background is the TSX/TDX DEM. Glacier ~~snout~~ positions are based on Landsat imagery. Location is shown in Fig. 2a.

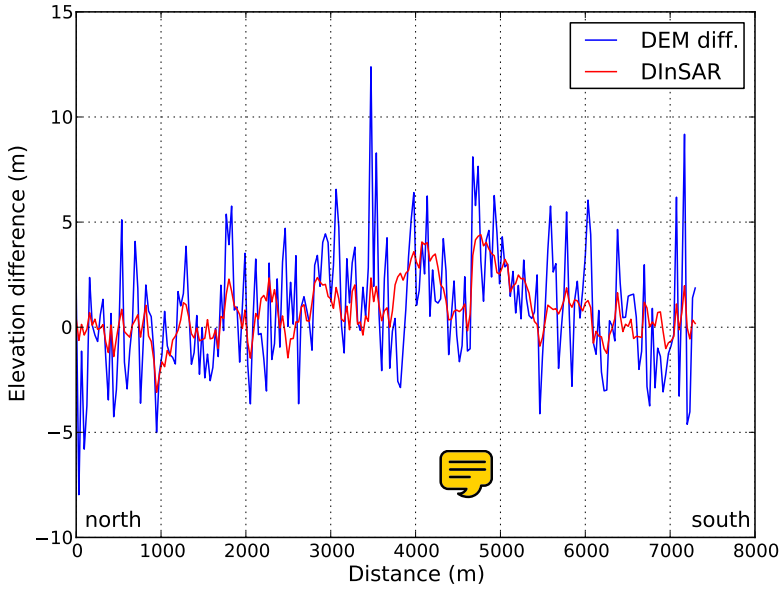

Fig. 5. Elevation changes along-track the SRTM-X flight path estimated with both methods (profile line is shown in Fig. 2b). Linear cross-track features may be related to attitude jitter of the space shuttle.